International Journal of Fluid Mechanics & Thermal Sciences
2026; 12(3): 62-75
http://www.sciencepublishinggroup.com/j/ijfmts
doi: 10.11648/j.ijfmts.20261203.12

Effect of Buoyancy Ratio on Double-Diffusive Natural Convection Flow in a Rectangular Enclosure

Peninnah Ngina Musili[1, *], Mark Okongo[2], Alice Lunani Mulama Murwayi[2]

[1]Faculty of Science and Technology, Chuka University, Meru, Kenya
[2]Department of Physical Sciences, Chuka University, Chuka, Kenya

Email address:

nginapenninah@gmail.com (Peninnah Ngina Musili), marikookongo@gmail.com (Mark Okongo), almurwayi@yahoo.com (Alice Lunani Mulama Murwayi)

To cite this article:

Peninnah Ngina Musili, Mark Okongo, Alice Lunani Mulama Murwayi. (2026). Effect of Buoyancy Ratio on Double-Diffusive Natural Convection Flow in a Rectangular Enclosure. *International Journal of Fluid Mechanics & Thermal Sciences, 12*(3), 62-75.
https://doi.org/10.11648/j.ijfmts.20261203.12

Received: 4 June 2026; **Accepted:** 23 June 2026 **Published:** 9 September 2026

Abstract: Double diffusive natural convection driven by Simultaneous temperature and concentration gradients are fundamental to many engineering and environmental processes. The buoyancy ratio N, defined as the ratio of solutal to thermal buoyancy forces, critically determines whether thermal or solutal effects dominate the flow structure, heat transfer, and species transport. While most existing studies rely on two-dimensional simplifications and alternative numerical methods, this paper presents a three-dimensional numerical investigation of the effect of the buoyancy ratio on steady, laminar double-diffusive natural convection in a rectangular enclosure with an aspect ratio of 0.5. The continuity, momentum, energy, and concentration equations governing the flow are solved using the finite-volume method with the SIMPLE algorithm on a staggered grid. Parametric simulations are performed for buoyancy ratios $N = 1.0, 2.5, 5.0$, and 10.0, with fixed Prandtl number $Pr = 7.0$, Lewis number $Le = 2.5$, and Rayleigh number $Ra = 50000$. Results show that increasing the buoyancy ratio from 1.0 to 10.0 significantly enhances the uniformity of the temperature field and enhances vertical heat transfer. Concentration profiles become sharper and more localized as the buoyancy ratio is increased. At a high buoyancy ratio, solutal buoyancy dominates, producing a thin solutal boundary layer and strong stratification, thereby promoting salt fingering. Velocity profiles become stronger, more organized, and more stable as the buoyancy ratio increases. The 3-dimensional nature of the flow reveals that the effect of the buoyancy ratio in the enclosure is isotropic; the primary circulation plane along the z-y plane shows the greatest changes, while the secondary planes (x-y and x-z) show only a significant change. The finite volume method proves to be an effective tool for 3-dimensional parametric studies. The results provide a valuable benchmark for engineering applications where controlling the balance between thermal and solutal buoyancy is crucial, such as chemical reactors, drying systems, and thermal management devices.

Keywords: Buoyancy Ratio, Double-Diffusive Convection, Finite Volume Method, 3-D Flow, Heat and Mass Transfer

1. Introduction

Convection is a mode of heat transfer that occurs when a fluid flows over a solid surface of different temperature. When buoyancy forces arise from both temperature and concentration gradients, the phenomenon is termed double diffusive natural convection, also called thermal-solute convection. This process is central to many applications, including oceanography (salt fingers), building ventilation, the drying of agricultural products, the cooling of electronic devices, and chemical processing.

The buoyancy ratio N is mathematically defined by equation (1)

$$N = \frac{\beta_c(C_h - C_l)}{\beta_T(T_h - T_l)}, \tag{1}$$

where β_T and β_c are the thermal and solutal expansion coefficients, and ΔT and ΔC are the imposed temperature and concentration differences. The value of N determines the relative strength and direction of the two buoyancy mechanisms:

1) $N > 1$: solutal buoyancy dominates, often leading to layered convection or salt fingering.
2) $N < 1$: thermal buoyancy dominates, yielding more stable, uniform convection.
3) $N = 1$: thermal and solutal effects are comparable, resulting in complex flow interactions.

Early research on double-diffusive convection established the importance of dimensionless parameters such as buoyancy ratio (Veronis [1] and Turner [2]). Subsequent studies have explored the role of buoyancy ratio N in various enclosures.

Mamou et al [4] analytically and numerically studied double-diffusive convection in a vertical rectangular enclosure. They derived that the buoyancy ratio determines the direction (aiding or opposing) and strength of thermal and solutal buoyancy forces. When thermal and solutal forces act in the same direction (reinforcing each other), convection is enhanced; when they act in opposite directions, convection may be suppressed, leading to layered flow structures. Their numerical solutions using the finite difference method showed good agreement with analytical predictions.

Nishimura et al [5] investigated oscillatory double-diffusive convection in a rectangular enclosure with opposing horizontal temperature and concentration gradients. For $Ra_T = 10^5$, $Pr = 1$, $Le = 2$, and $AR = 2$ [2]. They observed that oscillatory flow occurred only within a certain range of buoyancy ratio ($N = 0.02$ to 2.0). Their Crank?Nicolson scheme captured the transition from steady to oscillatory convection, but the study remained two-dimensional.

Ridha and Mounir[13] studied double-diffusive mixed convection in a double-lid driven rectangular cavity using the finite volume method [3]. They varied the buoyancy ratio and the Rayleigh number and found that increasing N increased the temperature and enhanced convection-driven heat transfer. At $Ra = 10^6$, the effect was most pronounced. Their work employed the FVM but was limited to two-dimensional geometry.

Koufi et al [16] performed a three-dimensional study of double-diffusive natural convection in a cavity filled with an air-CO_2 mixture, using the finite volume method with the SIMPLEC algorithm [4]. They reported that for positive buoyancy ratios, thermal and solutal forces cooperate; for $N = 0$, solutal forces are weak and the flow is purely thermoconvective; for large negative N, competition occurs. Their work is one of the few 3D studies, but they did not systematically vary N above 1.0; the present study extends to $N = 10.0$.

Xu et al.[17] applied lattice Boltzmann simulations to double-diffusive natural convection in an enclosure, considering Soret and Dufour effects [5]. They found that heat and mass transfer were weakened as the Dufour and Soret numbers increased, while varying the buoyancy ratio between -10 and 10. However, their method differed from FVM, and the geometry was two-dimensional.

Despite these valuable contributions to the literature, a systematic three-dimensional parametric study of the buoyancy ratio using the finite-volume method remains lacking, especially for $N > 1$ where solutal buoyancy dominates [8, 14, 15] for the lack of a 3D study [6, 7, 9, 12]. While previous studies, including Belazizia et al. [11], have explored double-diffusive natural convection, most have focused on 2D geometries or different boundary conditions. The current paper addresses this gap by focusing exclusively on the buoyancy ratio, using a full 3-dimensional finite-volume method (FVM) and analyzing results across three orthogonal planes. While many studies, including Aghighi et al. [18], address double-diffusive natural convection, especially for Newtonian fluids in a rectangular enclosure, these studies remain limited, justifying the present study's focus.

This paper focuses specifically on the effect of varying buoyancy ratio on concentration, temperature, and velocity profiles in a steady, laminar, 3-dimensional double-diffusive natural convection in a rectangular enclosure.

2. Mathematical Formulation and Methodology

2.1. Physical Model and Assumptions

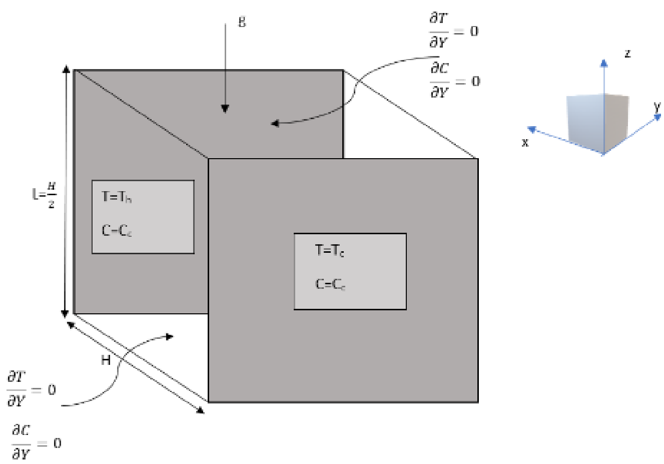

Figure 1. Physical model

The physical model of the flow problem, figure 1, is a rectangular enclosure of aspect ratio $AR = 0.5$, height L, width, and depth scaled accordingly as depicted in Figure 1. The left vertical wall ($x = 0$) is maintained at constant high temperature T_h and high concentration C_h. The opposite vertical wall ($x = W$) is at constant low temperature T_l and low concentration C_l. All other walls are adiabatic and impermeable. Gravity acts vertically downward (negative z-direction). The working fluid is a water-salt mixture.

The following assumptions are made:

1) The flow is three-dimensional, steady, and laminar.
2) The fluid is in-compressible.
3) Gravitational acceleration acts only in the z-direction.
4) The Boussinesq approximation holds: density is constant

except in the buoyancy term given by equation (2)

$$\rho = 1 - \beta_T(T_h - T_l) + \beta_s(C_h - C_l) \tag{2}$$

5) Dufour and Soret effects are negligible.

These boundary conditions and assumptions are applied to the general equations of continuity,momentum, energy and concentration equations to obtain the specific equations that model the flow in this study.

2.2. Governing Equations

The specific equations modeling the flow are non-dimensionalized using characteristic scales (length L, velocity U_0, temperature difference $\Delta T = T_h - T_l$, concentration difference $\Delta C = C_h - C_l$) to yield the dimensionless governing equations given by (3) to (8) Anderson et al [10]

Continuity:

$$\frac{\partial u}{\partial x} + \frac{\partial v}{\partial y} + \frac{\partial w}{\partial z} = 0 \tag{3}$$

X-momentum:

$$u\frac{\partial u}{\partial x} + v\frac{\partial u}{\partial y} + w\frac{\partial u}{\partial z} = -\frac{\partial p}{\partial x} + \frac{1}{Pr}\nabla^2 u \tag{4}$$

Y-momentum:

$$u\frac{\partial v}{\partial x} + v\frac{\partial v}{\partial y} + w\frac{\partial v}{\partial z} = -\frac{\partial p}{\partial y} + \frac{1}{Pr}\nabla^2 v \tag{5}$$

Z-momentum (includes buoyancy):

$$u\frac{\partial w}{\partial x} + v\frac{\partial w}{\partial y} + w\frac{\partial w}{\partial z} = -\frac{\partial p}{\partial z} + \frac{1}{Pr}\nabla^2 w + \frac{Ra}{Pr}(\theta - NC) \tag{6}$$

Energy:

$$u\frac{\partial \theta}{\partial x} + v\frac{\partial \theta}{\partial y} + w\frac{\partial \theta}{\partial z} = \frac{1}{Pr}\nabla^2 \theta \tag{7}$$

Concentration:

$$u\frac{\partial S}{\partial x} + v\frac{\partial S}{\partial y} + w\frac{\partial S}{\partial z} = \frac{1}{Le}\nabla^2 S \tag{8}$$

The dimensionless parameters are defined by equation (9) to (12)

$$Pr = \frac{\nu}{\alpha} \tag{9}$$

$$Ra = \frac{g\beta_T(T_h - T_l)L^3}{\alpha\nu} \tag{10}$$

$$Le = \frac{\alpha}{D} \tag{11}$$

$$N = \frac{\beta_c(C_h - C_l}{\beta_T(T_h - T_l} \tag{12}$$

2.3. Numerical Method

The governing partial differential equations are discretized using the finite volume method (FVM), which transforms the continuous equations into a system of algebraic equations by integrating over discrete control volumes. A key advantage of FVM is that it ensures conservation of mass, momentum, energy, and species over each control volume and hence over the entire domain.

2.3.1. Grid Generation and Staggered Arrangement

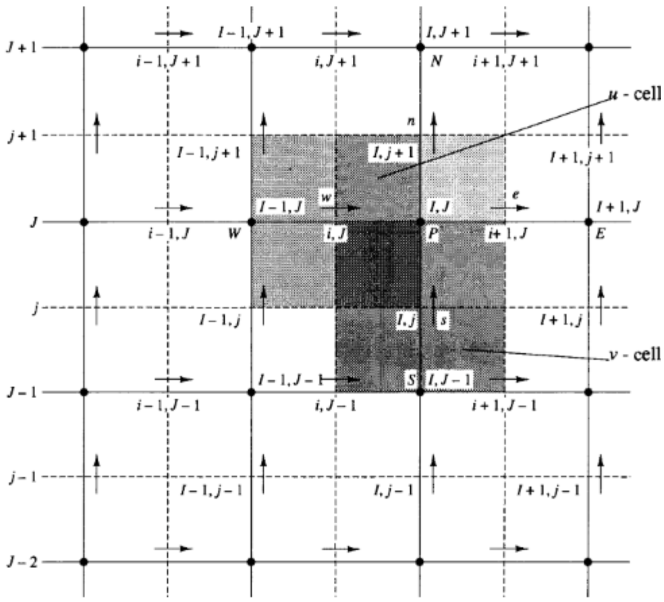

Figure 2. Discretization grid

The three-dimensional domain, figure 2 (dimensions $L_x = L_y = L_z$ with AR=0.5) is subdivided into uniform rectangular control volumes as depicted in figure 2. A general nodal point P is identified with its neighbors: East (E), West (W), North (N), South (S), Top (T), and Bottom (B). The control volume faces are denoted by lowercase letters e, w, n, s, t, b.

To avoid unphysical oscillatory pressure fields, a staggered grid is employed. The idea is to evaluate scalar variables at ordinary nodal points and velocity components at the staggered-grid points centered on the cell faces. In this study, Scalar variables (pressure p, temperature θ, concentration S) are stored at the main nodal points. Velocity components are stored on the cell faces: u velocities on the east and west faces, v velocities on the north and south faces, and w velocities on the top and bottom faces. This arrangement ensures that the pressure gradient driving a velocity component is evaluated across the same control volume for which that velocity is computed, providing a strong coupling between pressure and velocity.

2.3.2. Parameter Ranges

The following fixed parameters were used: $Ar = 0.5$, $Pr = 7.0$ (water-salt mixture), $Le = 2.5$, $N = 10$. The Rayleigh number was varied in a range that spans the conduction-dominated regime ($Ra = 10^4$), the transition regime ($Ra = 5 \times 10^4$), and the convection-dominated regime ($Ra = 10^5$ and 10^6), while remaining within laminar flow bounds ($Ra < 10^9$).

2.3.3. Discretization of the Transport Equations

Applying the finite volume method to the x-momentum equation (as an example) over the u-control volume and using central differencing for diffusive fluxes yields a discretized equation of the form:

$$a_P u_{i,J,K} = \sum a_{nb} u_{nb} + (P_{I,J,K} - P_{I-1,J,K}) A_{i,J}, \quad (13)$$

where the summation index nb runs over the six neighboring velocity nodes ($i \pm 1, J, K$; $i, J \pm 1, K$; $i, J, K \pm 1$). The coefficients a_{nb} contain contributions from convective and diffusive fluxes through the faces, and a_P is the sum of all neighboring coefficients plus any source terms. Similar discretized equations are obtained for the v- and w-momentum equations. The buoyancy term in the z-momentum equation becomes a source term that couples the temperature and concentration fields to the velocity field.

For the energy and concentration equations, which are scalar transport equations, the discretization is performed over the main (scalar) control volume, yielding:

$$a_P \phi_{I,J,K} = \sum a_{nb} \phi_{nb}, \quad (14)$$

where ϕ stands for θ or S. The coefficients depend on the velocity field, the Prandtl number (for energy), and the Lewis number (for concentration).

2.3.4. Pressure-Velocity Coupling: The SIMPLE Algorithm

The continuity equation does not contain an explicit pressure term. To link pressure and velocity, the Semi-Implicit Method for Pressure-Linked Equations (SIMPLE) algorithm is employed. The iterative procedure is as follows:

1) Guess the pressure field p^*.
2) Solve the momentum equations using p^* to obtain intermediate velocity components u^*, v^*, w^* from the discretized equations.
3) Compute pressure corrections p' such that $p = p^* + p'$. Velocity corrections u', v', w' are related to p' via simplified relations derived by dropping the neighboring velocity correction terms:

$$\begin{aligned} u' &= d_u(p'_{I-1,J,K} - p'_{I,J,K}), \\ v' &= d_v(p'_{I,J-1,K} - p'_{I,J,K}), \\ w' &= d_w(p'_{I,J,K-1} - p'_{I,J,K}). \end{aligned}$$

Here d_u, d_v, d_w are geometric coefficients from the momentum discretization.

4) Substitute the corrected velocities $u = u^* + u'$, etc., into the discretized continuity equation. This yields a Poisson-like equation for the pressure correction p':

$$\begin{aligned} a_{I,J,K} p'_{I,J,K} &= a_{i+1,J,K} p'_{I+1,J,K} + a_{i-1,J,K} p'_{I-1,J,K} \\ &+ a_{I,j+1,K} p'_{I,J+1,K} + a_{I,j-1,K} p'_{I,J-1,K} \\ &+ a_{I,J,k+1} p'_{I,J,K+1} + a_{I,J,k-1} p'_{I,J,K-1} + b_{I,J,K}, \end{aligned}$$

where the source term b contains the mass imbalance from the guessed velocities.

5) Solve the pressure correction equation (using a tri-diagonal matrix algorithm line by line) to obtain p'.
6) Update pressure and velocities: $p = p^* + \alpha_p p'$, $u = u^* + d_u(p'_{I-1,J,K} - p'_{I,J,K})$, etc., where α_p is an under-relaxation factor (typically 0.8 for pressure).
7) Solve the energy and concentration equations using the updated velocity field.
8) Check convergence: If residuals are above a tolerance (here 10^{-6}), return to step 2 with the corrected pressure as the new guess.

2.3.5. The Final Set of Discretized Equations

The final set of the dicretized momentum, energy, concentration and corrected presure equations are given by equations 15 to 20

1) the x-momentum equation

$$\begin{aligned} a_P U_{i,J,K} &= a_E U_{i+1,J,K} + a_W U_{i-1,J,K} \\ &+ a_N U_{i,J+1,K} + a_S U_{i,J-1,K} \\ &+ a_T U_{i,J,K+1} + a_B U_{i,J,K-1} \\ &+ P_{I,J,K} - P_{I-1,J,K} \end{aligned} \quad (15)$$

2) The y-momentum equation is given by equation

$$\begin{aligned} a_P V_{I,j,K} &= a_E V_{I+1,j,K} + a_W V_{I-1,j,K} \\ &+ a_N V_{I,j+1,K} + a_S V_{I,j-1,K} \\ &+ a_T V_{I,j,K+1} + a_B V_{I,j,K-1} \\ &+ P_{I,J,K} - P_{I,J-1,K} \end{aligned} \quad (16)$$

3) The z-momentum equation is given by equation

$$\begin{aligned} a_P W_{I,J} &= a_E W_{I+1,J,k} \\ &+ a_W W_{I-1,J,k} + a_N W_{I,J+1,k} \\ &+ a_S W_{I,J-1,k} + a_T W_{I,J,k+1} \\ &+ a_B W_{I,J,k-1} + P_{I,J,K} \\ &- P_{I,J,K-1} + b_{I,J,k} \end{aligned} \quad (17)$$

4) The energy equation is given by equation

$$\begin{aligned} a_P \theta_{I,J,K} &= a_E \theta_{I+1,J,K} + a_W \theta_{I-1,J,K} \\ &+ a_N \theta_{I,J+1,K} + a_S \theta_{I,J-1,K} \\ &+ a_T \theta_{I,J,K+1} + a_B \theta_{I,J,K-1} \end{aligned} \quad (18)$$

5) The concentration equation is given by equation

$$\begin{aligned} a_P S_{I,J,K} &= a_E S_{I+1,J,K} + a_W S_{I-1,J,K} \\ &+ a_N S_{I,J+1,K} + a_S S_{I,J-1,K} \\ &+ a_T S_{I,J,K+1} + a_B S_{I,J,K-1} \end{aligned} \quad (19)$$

6) The corrected pressure equation is given by equation

$$
\begin{aligned}
a_{i,j,k} P^{/}_{I,J,K} = a_{i+1,J,K} P^{/}_{I+1,J,K} \\
- a_{i-1,J,K} P^{/}_{I-1,J,K} \\
+ a_{I,j+1,K} P^{/}_{I,J+1,K} \\
- a_{I,j-1,K} P^{/}_{I,J-1,K} \\
+ a_{I,J,k+1} P^{/}_{I,J,K+1} \\
- a_{I,J,k-1} P^{/}_{I,J,K-1} \\
+ b_{I,J,K}
\end{aligned} \tag{20}
$$

The algorithm is implemented in MATLAB. Under-relaxation is applied to all variables to ensure stability. The solution is considered converged when the normalized residuals for all equations fall below 10^{-6}. Grid independence was verified by refining the mesh from $30 \times 30 \times 30$ to $50 \times 50 \times 50$ and monitoring changes in the Nusselt and Sherwood numbers (less than 2% variation). The final results are presented and discused.

3. Results and Discussion

3.1. Effect of Buoyancy Ratio on Temperature Profiles

3.1.1. Along the x-y Plane

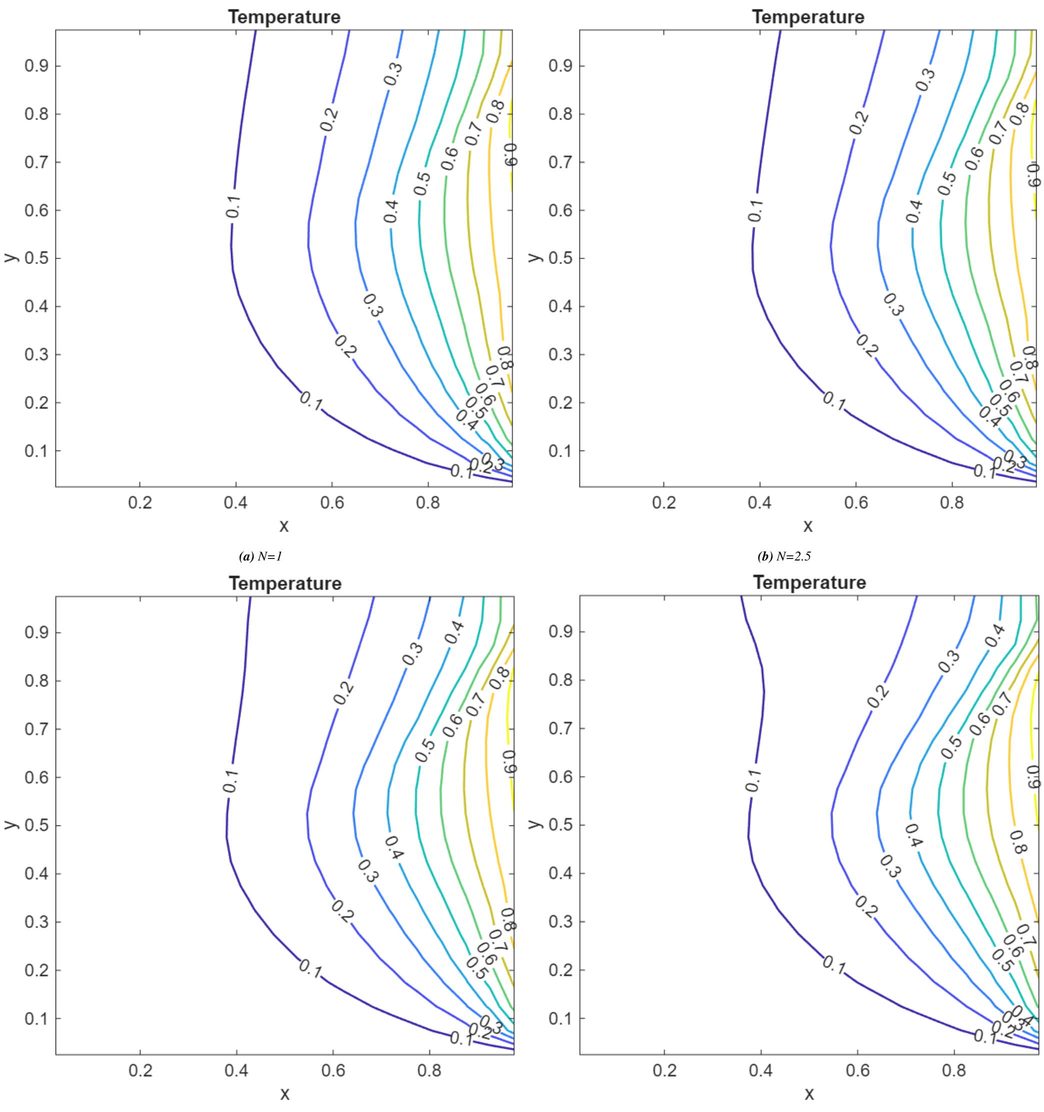

(a) N=1 *(b) N=2.5* *(c) N=5.0* *(d) N=10.0*

Figure 3. *Effects of Buoyancy ratio on the temperature profile along x-y plane.*

Figure 3 illustrates the temperature profiles along the x-y plane for N-1.0, 2.5, 5.0, and 10.0. For all values, a clear temperature gradient exists from the heated x-plane to the cooler y-plane. At $N = 1.0$ (thermal buoyancy dominates), the isotherms are somewhat curved and closely spaced near the hot wall, indicating a strong thermal boundary layer. As N increases to 2.5, 5.0, and 10.0, the isotherms become smoother and more evenly spaced, indicating a more uniform temperature distribution. This occurs because solutal buoyancy adds to the thermal buoyancy, enhancing vertical mixing and spreading heat more evenly across the cavity. The results also show a noticeable vertical heat exchange: hot fluid rises from the lower region and cool fluid sinks. The strength of this vertical exchange increases with N, as solutal forces amplify the overall buoyancy.

3.1.2. Along the x-z Plane

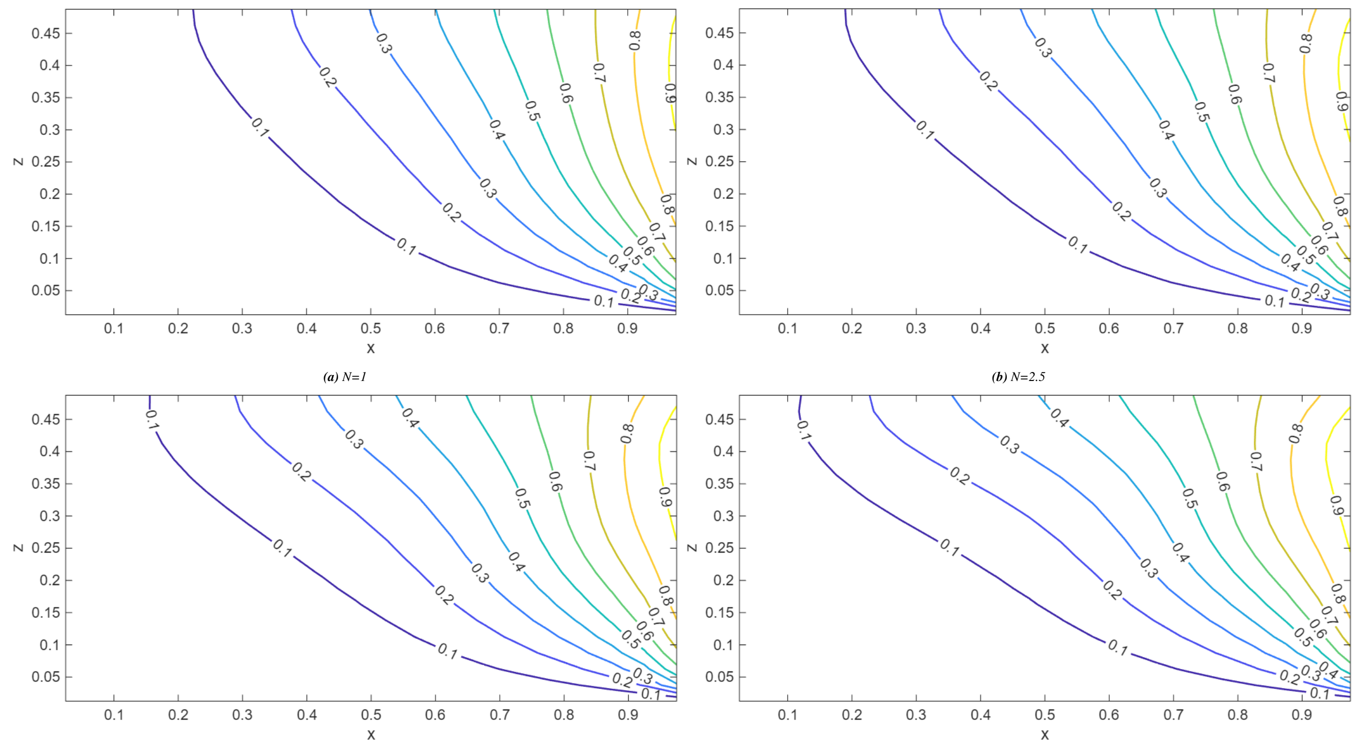

(a) N=1 *(b) N=2.5*

(c) N=5.0 *(d) N=10.0*

Figure 4. *Effect of Buoyancy ratio on the temperature profile along x-z plane.*

Figure 4 shows the temperature profiles along the x-z plane resulting from varying the buoyancy ratio. At low $N = 1.0$, the isotherms show strong vertical stratification, with hot fluid near the bottom and cold fluid near the top. As N increases, the isotherms become more uniformly distributed, especially in the upper part of the enclosure. This indicates that solutal buoyancy forces enhance vertical heat transfer, driving hot fluid higher and promoting mixing. At $N = 5.0$, the temperature field is nearly isothermal in the central region, demonstrating efficient heat distribution.

3.1.3. Along the z-y Plane

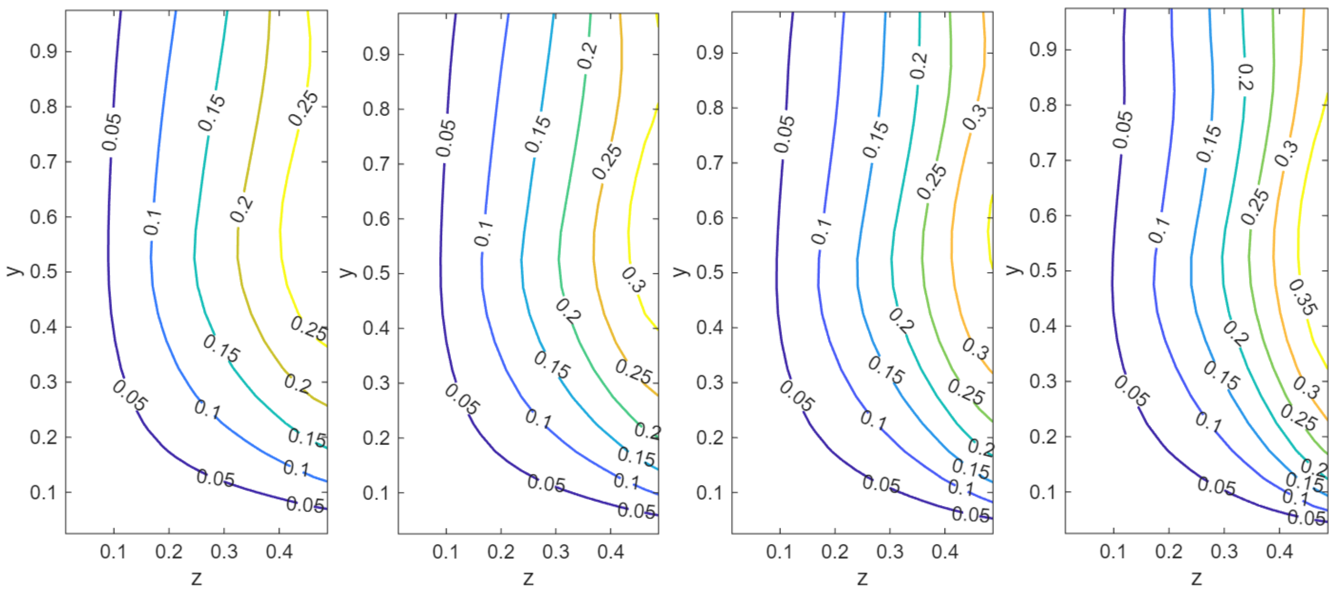

(a) N=1.0 (b) N=2.5 (c) N=5.0 (d) N=10

Figure 5. *Effect of Buoyancy ratio on the temperature profile along z-y plane.*

Figure 5 is a representation of the Buoyancy ratio on the temperature profiles along the vertical-lateral (z-y) plane in a double-diffusive natural convection system. The results are represented as isotherm contours, which show the primary temperature profiles in the z-y plane. A clear gradient exists from the heated z-plane to the cooler y-plane. At higher N, the isotherms become more evenly spaced, and the thermal boundary layer near the hot wall becomes thinner, indicating stronger convective heat transfer. The vertical heat exchange becomes more pronounced as N increases, with the hottest fluid rising to the top and cool fluid sinking to the bottom in a well-organized circulation cell. This aligns with Koufi et al [16], who observed that positive buoyancy ratios (cooperative forces) produce stronger thermal convection.

3.2. Effect of Buoyancy Ratio on Concentration Profiles

3.2.1. Along the x-y Plane

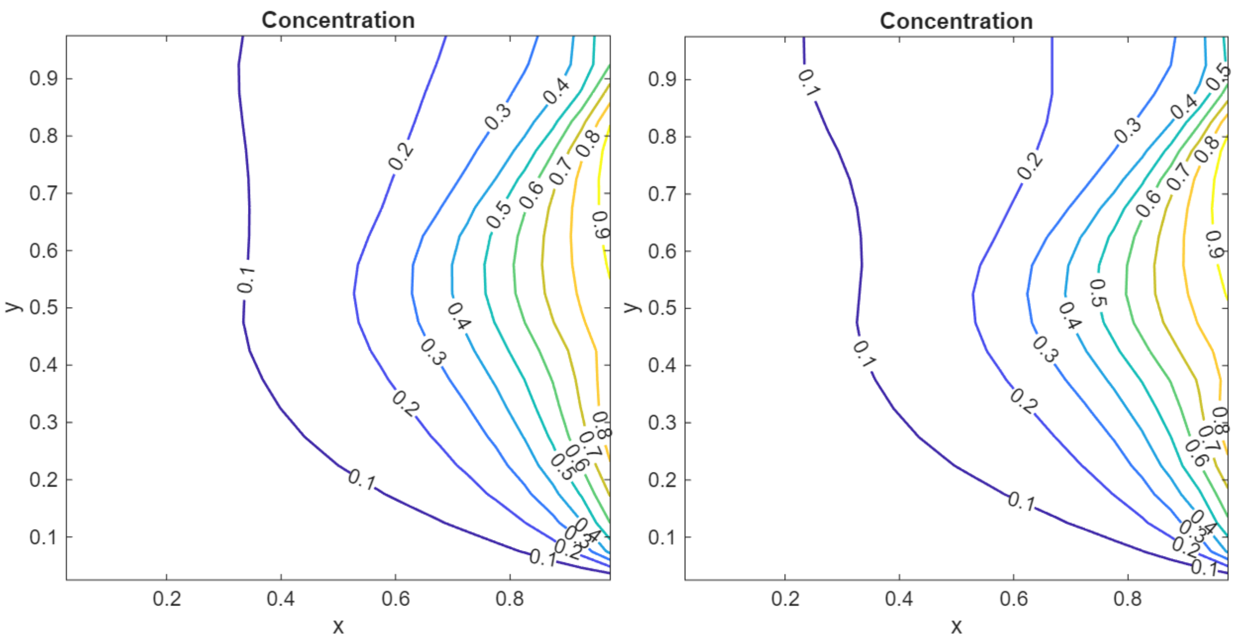

(a) N=1.0 (b) N=2.5

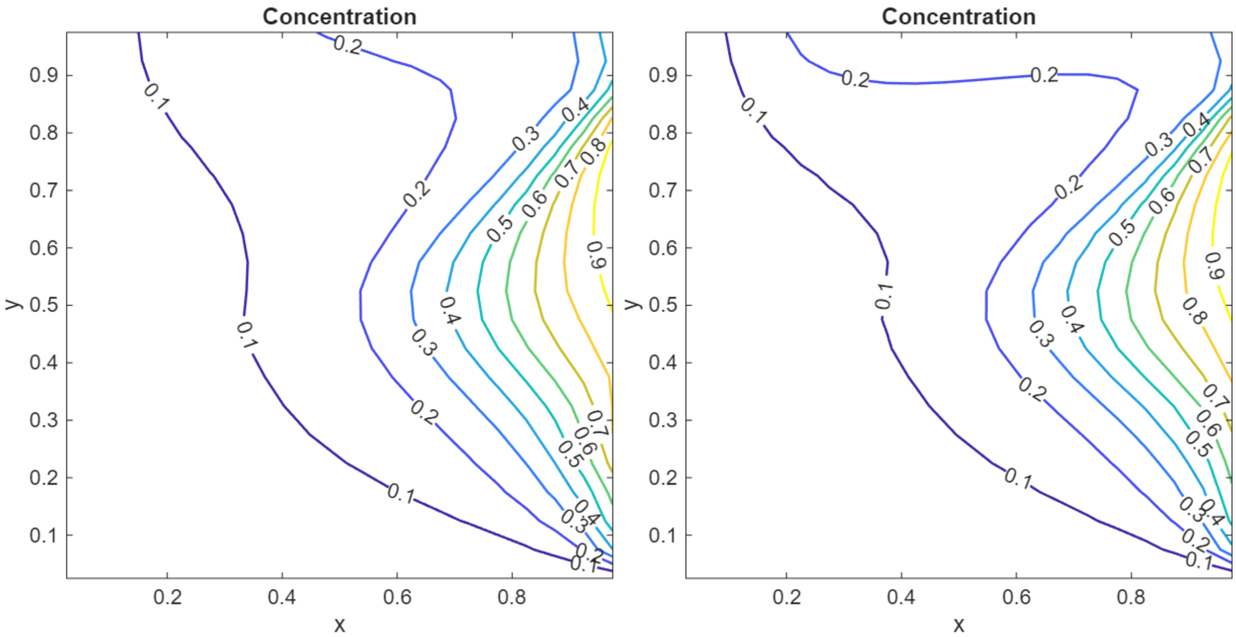

***(c)** N=5.0* ***(d)** N=10*

Figure 6. *Effect of Buoyancy ratio on the concentration profile along x-y plane.*

Figure 6 is a representation of the effect of varying buoyancy ratio on the concentration profiles along the horizontal- lateral (x-y) plane in an enclosure with double diffusive natural convection. The results shows iso-concentration lines on the x-y plane. At $N = 1.0$, thermal buoyancy dominates, and the concentration gradients are relatively smooth; the solute diffuses widely. As N increases to 2.5 and 5.0, solutal buoyancy becomes more important, and the iso-concentration lines become sharper, indicating thinner solutal boundary layers. At $N = 10.0$, the contours are tightly packed near the high-concentration wall, showing that solutal buoyancy dominates and strongly localizes the solute near the source. This is because the increased N enhances the solutal driving force, causing more vigorous solutal circulation and steeper gradients.

3.2.2. Along the x-z Plane

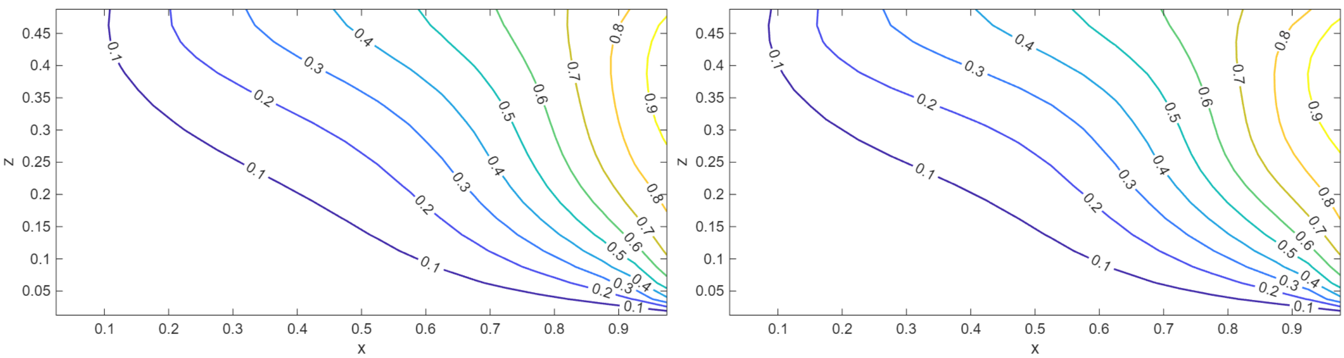

***(a)** N=1.0* ***(b)** N=2.5*

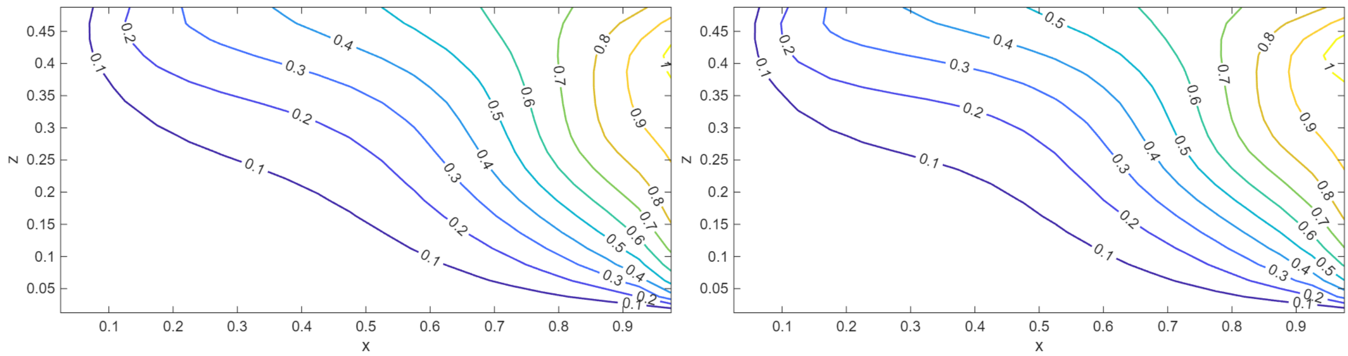

(c) N=5.0 *(d) N=10.0*

Figure 7. *Effect of Buoyancy ratio on the concentration profiles along x-z plane.*

Figure 7 is a representation of the effect of varying buoyancy ratio on the concentration profiles along the horizontal- vertical (x-z) plane in an enclosure with double diffusive natural convection. The fluid flow in the enclosure is driven by a combined temperature and concentration gradient. The results are represented using iso-concentration lines, which connect points of equal species concentration within the enclosure.Results illustrates concentration profiles along the x-z plane. At low N, the solute plume is wide and diffuses far into the cavity. As N increases, the plume becomes narrower and more vertical, with sharper concentration gradients. This indicates that solutal buoyancy forces drive stronger vertical transport, but the solute remains confined to a thinner layer near the hot wall. The secondary solutal circulation patterns become more pronounced at higher N.

3.2.3. Along the z-y Plane

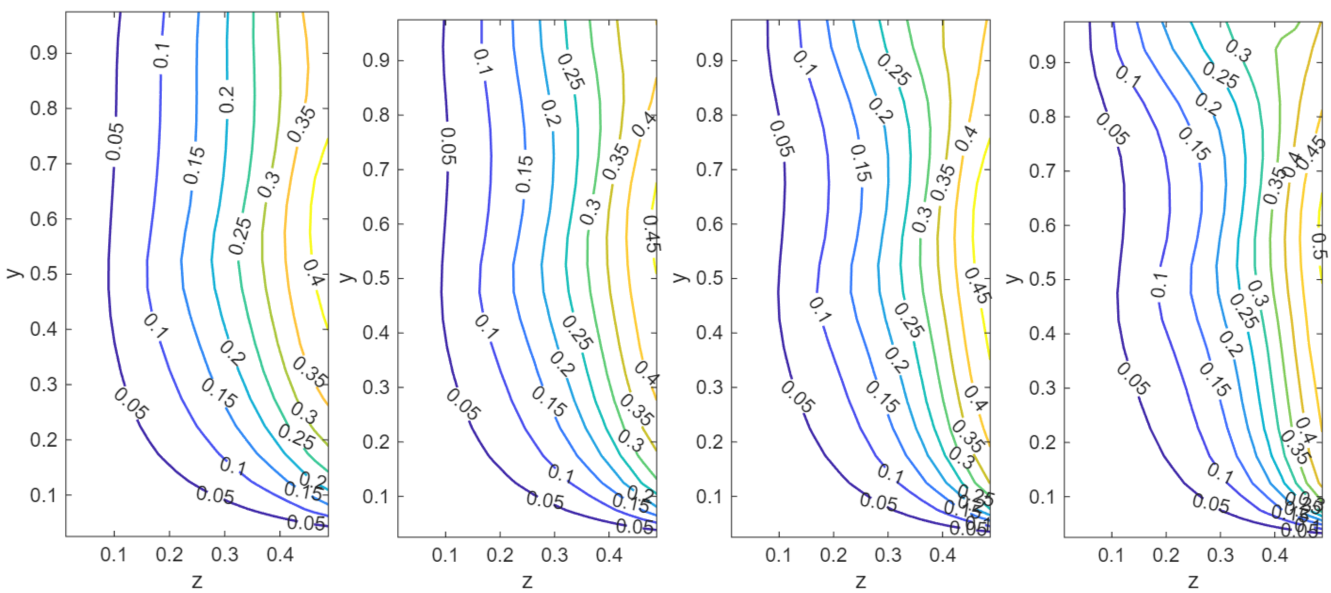

(a) N=1.0 *(b) N=2.5* *(c) N=5.0* *(d) N=10.0*

Figure 8. *Effect of Buoyancy ratio on the concentration profile along the z-y plane.*

Figure 8 is a representation of the effect of varying Buoyancy ratio on the concentration profiles along the vertical-lateral (z-y) plane in an enclosure with double diffusive natural convection. The fluid flow in the enclosure is driven by a combined temperature and concentration gradient. The results are represented using iso- concentration lines, which connect points of equal species concentration within the enclosure. The results show the concentration profiles along the z-y plane. Primary solutal transport occurs from the high-concentration z-plane to the low-concentration y-plane. At $N = 1.0$, the iso-concentration lines are widely spaced, indicating gradual mixing. As N increases to 10.0, the contours become much steeper and more distinct, with solute confined to a narrow region near the source. This implies that when solutal buoyancy dominates, the solute stratifies strongly and does not mix readily with the rest of the fluid. This behavior is typical of salt-fingering regimes when $N > 1$. These results are consistent with Nishimura et al [5] and extend their observations to 3-D.

3.3. Effect of Buoyancy Ratio on Velocity Profiles

3.3.1. Along the x-y Plane

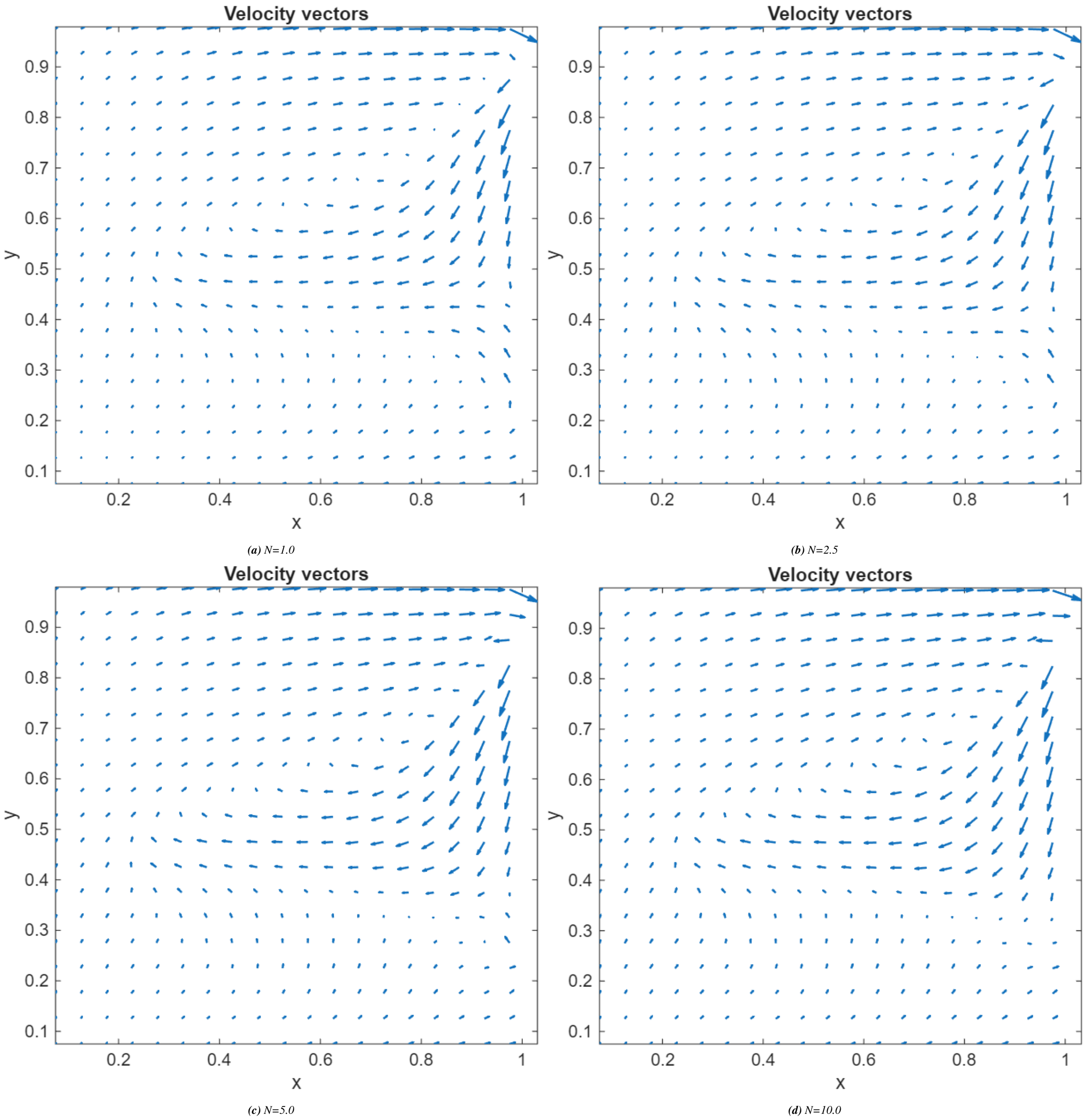

Figure 9. *Effect of Buoyancy ratio number on the velocity vector along x-y plane.*

Figure 9 is a vector plot of the effect of varying the Buoyancy ratio on the velocity profiles along the horizontal-vertical (x-y) plane in an enclosure with double-diffusive natural convection. The results are represented using iso-concentrates, which depict the direction and magnitude of fluid flow within the enclosure. The figure shows the direction and magnitude of fluid flow within the enclosure. The velocity profiles reveal the formation of secondary circulation within the enclosure. This circulation is driven by buoyancy forces resulting from simultaneous temperature and concentration gradients. Results show that secondary circulation is weak and disorganized, with vectors short and somewhat random. As N increases to 2.5, 5.0, and 10.0, the flow becomes increasingly organized and strong. At $N = 10.0$, well-defined circulation cells appear, with fluid moving from the hot wall toward the cold wall along the top and returning along the bottom. The maximum velocity magnitude increases significantly with N, indicating that solutal buoyancy enhances the overall flow strength. The flow also becomes more streamlined, suggesting improved stability.

3.3.2. Along the x-z Plane

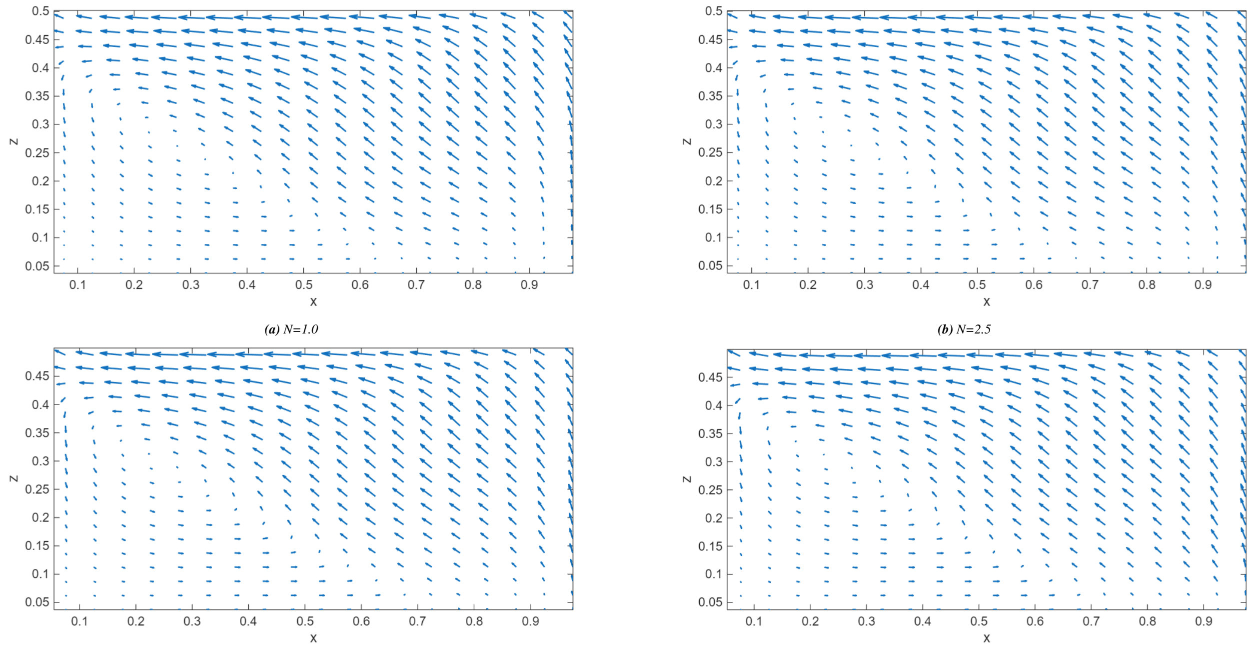

(a) N=1.0 *(b) N=2.5* *(c) N=5.0* *(d) N=10.0*

Figure 10. *Effect of Buoyancy ratio number on the velocity vector along x-z plane.*

Figure 10 is a vector plot of the effect of varying the Buoyancy ratio on the velocity profiles along the horizontal-vertical (x-z) plane in an enclosure with double-diffusive natural convection. The results are represented using iso-concentrates, which depict the direction and magnitude of fluid flow within the enclosure. The figure shows the direction and magnitude of fluid flow within the enclosure. The velocity profiles reveal the formation of secondary circulation within the enclosure. This circulation is driven by buoyancy forces resulting from simultaneous temperature and concentration gradients. Results reveal that at low N, vertical motion is weak, and the flow is nearly parallel to the horizontal direction. As N increases, a strong vertical circulation develops: hot fluid rises along the hot z-plane, moves horizontally toward the cold x-plane at the top, sinks along the cold wall, and returns along the bottom. This convection cell becomes more vigorous and compact at higher N. The vertical velocities increase markedly, enhancing mixing and heat transfer.

3.3.3. Along the z-y Plane

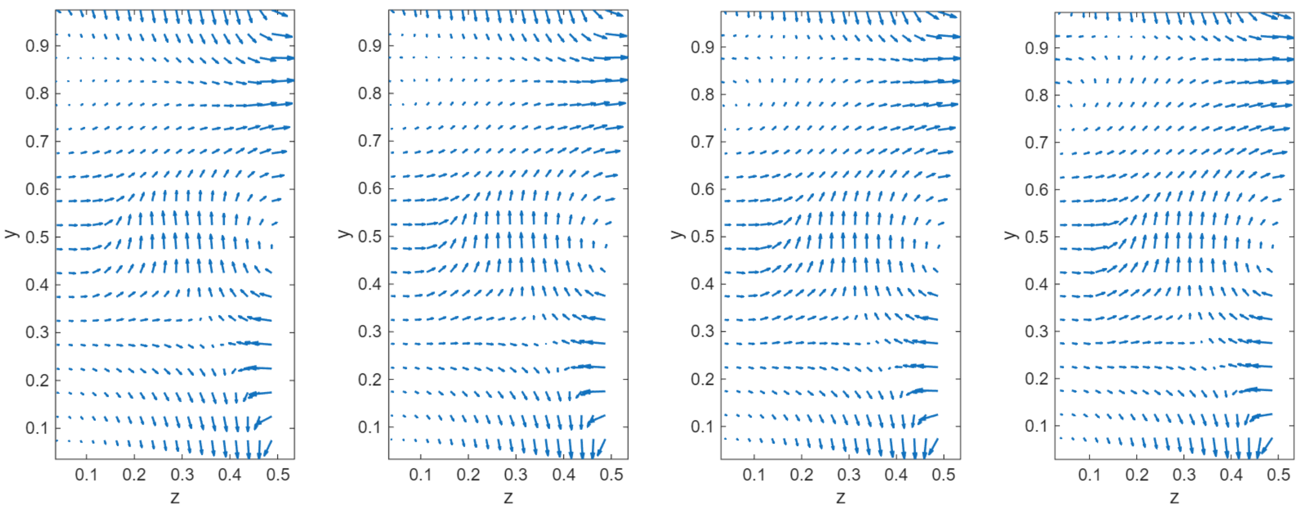

(a) N=1.0 *(b) N=2.5* *(c) N=5.0* *(d) N=10.0*

Figure 11. *Effect of Buoyancy ratio number on the velocity vector along z-y plane.*

Figure 11 is a vector plot of the effect of varying the Buoyancy ratio on the velocity profiles along the horizontal-vertical (z-y) plane in an enclosure with double-diffusive natural convection. The results are represented using iso-concentrates, which depict the direction and magnitude of fluid flow within the enclosure. The figure shows the direction and magnitude of fluid flow within the enclosure. The velocity profiles reveal the formation of secondary circulation within the enclosure. This circulation is driven by buoyancy forces resulting from simultaneous temperature and concentration gradients. The results illustrate the primary velocity field on the z-y plane. At $N = 1.0$, a single, weak circulation cell occupies the enclosure. As N increases, the circulation strengthens, and the cell becomes more elongated in the vertical direction. At $N = 10.0$, the flow is highly organized with intense upwelling along the hot wall and downwelling along the cold wall. The velocity vectors are longer and more uniform in direction, indicating a strong, stable convection regime dominated by solutal buoyancy.

These velocity observations are in excellent agreement with Ridha, B., & Mounir [13] and Koufi et al. [16], who reported that increasing the buoyancy ratio enhances circulation intensity. The present 3-D results further show that this enhancement is anisotropic: the effect is most pronounced in the primary circulation plane (z-y) and is also significant in the secondary planes (x-y and x-z).

3.4. Summary of Buoyancy Ratio Effects

1) *Temperature:* Higher N produces more uniform temperature distributions and enhanced vertical heat transfer. Isotherms become smoother and more evenly spaced.
2) *Concentration:* Higher N leads to sharper concentration gradients and more confined solute layers. Solutal buoyancy dominates at $N = 10.0$, creating strong stratification.
3) *Velocity:* Higher N results in stronger, more organized, and more stable circulation. Flow patterns evolve from weak, disorganized motions to vigorous, well-defined convection cells.

These effects are consistent with the physical interpretation: as the buoyancy ratio increases, solutal forces become progressively more important, augmenting the total buoyancy force and driving stronger convection.

4. Conclusion

This paper presents a three-dimensional numerical study of the effect of the buoyancy ratio N on temperature, concentration, and velocity profiles in steady, laminar double-diffusive natural convection within a rectangular enclosure (AR = 0.5). The finite volume method with SIMPLE algorithm was used to solve the coupled governing equations. The main conclusions are:

1) Increasing the buoyancy ratio from 1.0 to 10.0 significantly enhances the uniformity of the temperature field and increases vertical heat transfer. At $N = 10.0$, the temperature distribution is nearly isothermal in the core region.
2) Concentration profiles become sharper and more localized as N increases. At high N, solutal buoyancy dominates, producing thin solutal boundary layers and strong stratification, which may promote salt-fingering behavior.
3) Velocity fields become stronger, more organized, and more stable with increasing N. At $N = 10.0$, well-defined primary and secondary circulation cells develop, with maximum velocities several times higher than at $N = 1.0$.
4) The 3D nature of the flow reveals that the effect of N is anisotropic: the primary circulation plane (z-y) shows the strongest response, but secondary planes (x-y, x-z) also exhibit significant changes.

These results provide valuable benchmarks for engineering applications where controlling the balance between thermal and solutal buoyancy is crucial, such as in chemical reactors, drying systems, and thermal management devices. The finite volume method proves to be an effective tool for such 3-D parametric studies.

Future work should extend the analysis to unsteady and turbulent regimes, include Soret and Dufour effects, and explore negative buoyancy ratios (opposing flows) to fully characterize the dynamics of double-diffusive convection.

ORCID

0009-0001-0901-7381 (Peninnah Ngina Musili)

Abbreviations

MATLAB	Matrix Laboratory
FVM	Finite Volume Method
AR	Aspect Ratio
Cp	Specific Heat Capacity at Constant Pressure $jKg^{-1}K^{-1}$
g	Gravitational Acceleration ms^{-1}
T	Temperature K
P	Thermodynamic Pressure Nm^2
t	Time s
h	Hot Wall and High Concentration
c	Cold Wall and Low Concentration
u, v	Velocity Components
x, y	Dimensional Coordinates
Pr	Prandtl Non-dimensional Number
Ra	Rayleigh Non-dimensional Number
Sc	Schmidt Non-dimensional Number
Le	Lewis Non-dimensional Number
α	Thermal Diffusivity m^2s^{-1}
ρ	Density Kgm^{-3}
υ	Kinematic Viscosity m^2s^{-1}

β Thermal Expansion Coefficient K^{-1}
D Mixture Average Diffusion Coefficient
λ Thermal Conductivity

Acknowledgments

The author gratefully acknowledge Chuka University for providing computational facilities and academic support. Special thanks to colleagues in the Department of Physical Sciences for constructive discussions that enriched this work.

Authors Contribution

Peninnah Ngina Musili: Conceptualization, Formal Analysis, Methodology, Software Visualization, Writing – original draft, Writing – review & editing

Mark Okongo: Project administration, Supervision, Validation

Alice Lunani Mulama Murwayi: Project administration, Supervision, Validation

Conflicts of Interest

The authors declare no conflict of interest.

References

[1] Veronis, G. (1965). On finite amplitude instability in thermohaline convection. *Journal of Marine Research*, 23, 1-17.

[2] Turner, J. S. (1965). Coupled turbulent transport of salt and heat across a sharp density interface. International Journal of Heat and Mass Transfer, 8(5), 759-767. https://doi.org/10.1016/0017-9310(65)90022-0

[3] Ho, C. J., & Chang, J. Y. (1994). A study of natural convection heat transfer in a vertical rectangular enclosure with two-dimensional discrete heating: Effect of aspect ratio. International Journal of Heat and Mass Transfer, 37(6), 917-925. https://doi.org/10.1016/0017-9310(94)90217-8

[4] Mamou, M., Vasseur, P., & Bilgen, E. (1996). Analytical and numerical study of double diffusive convection in a vertical enclosure. Heat and Mass Transfer, 32(1-2), 115-125. https://doi.org/10.1007/s002310050100

[5] Nishimura, T., Wakamatsu, M., & Morega, A. M. (1998). Oscillatory double-diffusive convection in a rectangular enclosure with combined horizontal temperature and concentration gradients. International Journal of Heat and Mass Transfer, 41(11), 1601-1611. https://doi.org/10.1016/S0017-9310(97)00201-6

[6] Mohamad, A. A., & Bennacer, R. (2002). Double-diffusion natural convection in an enclosure filled with a saturated porous medium. Numerical Heat Transfer, Part A: Applications, 41(5), 453-470. https://doi.org/10.1080/10407780290059564

[7] Costa, V. A. F. (2004). Double-diffusive natural convection in parallelogrammic enclosures. International Journal of Heat and Mass Transfer, 47(14-16), 2913-2926. https://doi.org/10.1016/j.ijheatmasstransfer.2004.02.013

[8] Abu-Nada, E., Masoud, Z., Oztop, H. F., & Campo, A. (2010). Effect of nanofluid variable properties on natural convection in enclosures. International Journal of Thermal Sciences, 49(3), 479-491. https://doi.org/10.1016/j.ijthermalsci.2010.07.006

[9] Kuznetsov, G. V., & Sheremet, M. A. (2011). Natural convection in an enclosure with double diffusive conjugate natural convection. International Journal of Heat and Mass Transfer, 54(1-3), 456-465. https://doi.org/10.1016/j.ijheatmasstransfer.2010.09.009

[10] ,Anderson, D., Tannehill, J. C., Pletcher, R. H., Munipalli, R., & Shankar, V. (2020). Computational Fluid Mechanics and Heat Transfer. CRC Press.

[11] Belazizia, A., Benissaad, S., & Abboudi, S. (2012). Double-diffusion natural convection of binary fluid in a square enclosure with top active vertical wall. *Advances in Theoretical and Applied Mechanics*, 5(3), 119-131.

[12] Elsherbiny, S. M., & Ragab, E. H. (2013). Laminar natural convection in inclined rectangular cavities with a localized heat source. Alexandria Engineering Jour- nal, 52(3), 249-257. https://doi.org/10.1016/j.aej.2012.12.004

[13] Ridha, B., & Mounir, B. (2014). Effect of buoyancy ratio on double-diffusive mixed convection in a double-lid driven rectangular cavity. Heat Transfer Engineering, 35(5), 456-467. https://doi.org/10.1080/01457632.2013.819539

[14] Falahat, A. (2014). Effect of aspect ratio on laminar natural convection in a partially heated enclosure. Universal J. Mech. Eng, 2(1), 28-33.

[15] Aly, A. M., & Raizah, Z. A. (2016). Double-diffusive natural convection in an enclosure filled with nanofluid using ISPH method. Alexandria Engineering Journal, 55(4), 3037-3052. https://doi.org/10.1016/j.aej.2016.07.004

[16] Koufi, L., Cherif, Y., Younsi, Z., & Naji, H. (2019). Double-diffusive natural convection in a mixture-filled cavity with walls' opposite temperatures and concentrations. Heat Transfer Engineering, 40(15), 1268-1285. https://doi.org/10.1080/01457632.2018.1457770

[17] Xu, H., Luo, Z., Lou, Q., Zhang, S., & Wang, J. (2019). Lattice Boltzmann simulations of the double-diffusive natural convection and oscillation characteristics in an enclosure with Soret and Dufour effects. International Journal of Thermal Sciences, 136, 159-171. https://doi.org/10.1016/j.ijthermalsci.2018.12.012

[18] Aghighi, M., Ammar, A., & Masoumi, H. (2022). Double-diffusive natural convection of Casson fluids in an enclosure. International Journal of Mechanical Sciences, 236, 107754. https://doi.org/10.1016/j.ijmecsci.2022.107754